Current Biology 21, 1720–1726, October 25, 2011 ©2011 Elsevier Ltd All rights reserved DOI 10.1016/j.cub.2011.08.057

Report

Pectin-Induced Changes in Cell Wall Mechanics Underlie Organ Initiation in *Arabidopsis*

Alexis Peaucelle,[1,2,5,*] Siobhan A. Braybrook,[3,5] Laurent Le Guillou,[4] Emeric Bron,[2,4] Cris Kuhlemeier,[3] and Herman Höfte[1,*]

[1]Institut Jean-Pierre Bourgin, UMR1318 INRA-AgroParisTech, 78026 Versailles, France

[2]Université Paris Diderot, UFR de Physique de Paris 7, 75205 Paris, France

[3]Institute of Plant Sciences, University of Bern, CH-3013 Bern, Switzerland

[4]Université Pierre et Marie Curie, Université Paris 06, UMR 7585, Laboratoire de Physique Nucléaire et des Hautes Energies, 75005 Paris, France

Summary

Tissue mechanics have been shown to play a key role in the regulation of morphogenesis in animals [1–4] and may have an equally important role in plants [5–9]. The aerial organs of plants are formed at the shoot apical meristem following a specific phyllotactic pattern [10]. The initiation of an organ from the meristem requires a highly localized irreversible surface deformation, which depends on the demethylesterification of cell wall pectins [11]. Here, we used atomic force microscopy (AFM) to investigate whether these chemical changes lead to changes in tissue mechanics. By mapping the viscoelasticity and elasticity in living meristems, we observed increases in tissue elasticity, correlated with pectin demethylesterification, in primordia and at the site of incipient organs. Measurements of tissue elasticity at various depths showed that, at the site of incipient primordia, the first increases occurred in subepidermal tissues. The results support the following causal sequence of events: (1) demethylesterification of pectin is triggered in subepidermal tissue layers, (2) this contributes to an increase in elasticity of these layers—the first observable mechanical event in organ initiation, and (3) the process propagates to the epidermis during the outgrowth of the organ.

Results

The Mechanical Properties of the Meristem: Viscoelasticity and Elasticity

In plants, organ emergence requires cell expansion, which is controlled by turgor pressure and wall relaxation [12, 13]. As such, organ emergence likely requires changes in wall mechanics as suggested by the triggering of ectopic organs by applying the wall-loosening agent expansin [14]. Manipulation of pectins within the cell walls of the meristem also affects organ emergence [11]. The plant cell wall can be considered as a fiber-reinforced composite: rigid cellulose microfibrils are embedded in, and crosslinked by, a hemicellulose and pectin matrix [15–17]. In the absence of growth (irreversible, or plastic, deformation), plant cell walls behave as a viscoelastic material—they retain shape after deformation, but with a time delay [18]. We first used atomic force microscopy (AFM) to examine the viscoelasticity of the meristem through relaxation time experiments. Using an AFM cantilever mounted with a 5 μm bead, we performed 20 s cyclical indentations at several positions on plasmolyzed meristems to study the tissue response (see Figure S1 available online). The data were fitted with a modified Kelvin-Voigt model, separating the behavior into two components: a bulk elastic constant and a relaxation time (Figure S1). The bulk elastic constant showed large variation between the meristem dome and the primordia (Figure 1A), whereas the relaxation time values did not differ significantly. The increased elasticity correlates with the higher growth and division rates in primordia compared to the meristem [19–21].

Changes in Tissue Mechanics Associated with Organ Initiation in the Apical Meristem

We next focused solely on the elastic component by increasing the speed of indentations to negate the viscous behavior (Figure S1). We used a Hertzian model to fit the indentation data and define the apparent Young's modulus (E_A, coefficient of elasticity) for the tissue [22] (Figure S1). The higher the E_A, the less elastic (or stiffer) the tissue is.

We mapped E_A on inflorescence meristems using a 5 μm diameter tip, which, as shown below, provided information from several cell layers of the meristem combined. We observed that E_A was lower in primordia (P2–P4) than in the meristem (Figures 1C and 1D; Figure S1). Surprisingly, the areas corresponding to the incipient primordia also showed lower E_A. Thus, decreases in E_A both preceded and accompanied organ emergence and correlated with an increased pectin demethylesterification [11]. The observed differences in E_A in principle may reflect several parameters: cell geometry, wall anisotropy, wall elasticity, or wall thickness. Because the decrease in E_A occurred without obvious changes in cell geometry (Figures 1E–1J) and did not correlate with the predicted degree of cellulose anisotropy in the outer tangential cell wall of the epidermal layer (see Supplemental Experimental Procedures) [7, 8], we conclude that it must reflect changes in wall elasticity and/or thickness.

Pectin Modification Alters Cell Wall Mechanics in Apical Meristems

We next focused on the role of pectin in cell wall mechanics. The degree of methylesterification of the pectic polymer homogalacturonan (HG) is directly related to its physicochemical properties [23]. HG is secreted in a highly methylesterified form and is selectively demethylesterified in the cell wall by pectin methylesterases (PMEs). PME activity is antagonized by endogenous PME inhibitors (PMEIs) [23].

We have shown that the overexpression of *PECTIN METHYLESTERASE 5* (*PME5oe*) leads to decreased pectin methylesterification and ectopic primordia, whereas overexpresssion of *PECTIN METHYLESTERASE INHIBITOR 3* (*PMEI3oe*) leads to increased pectin methylesterification and the inhibition of organ formation (Figures 2A and 2B) [11].

[5]These authors contributed equally to this work

*Correspondence: alexis.peaucelle@versailles.inra.fr (A.P.), herman.hofte@versailles.inra.fr (H.H.)

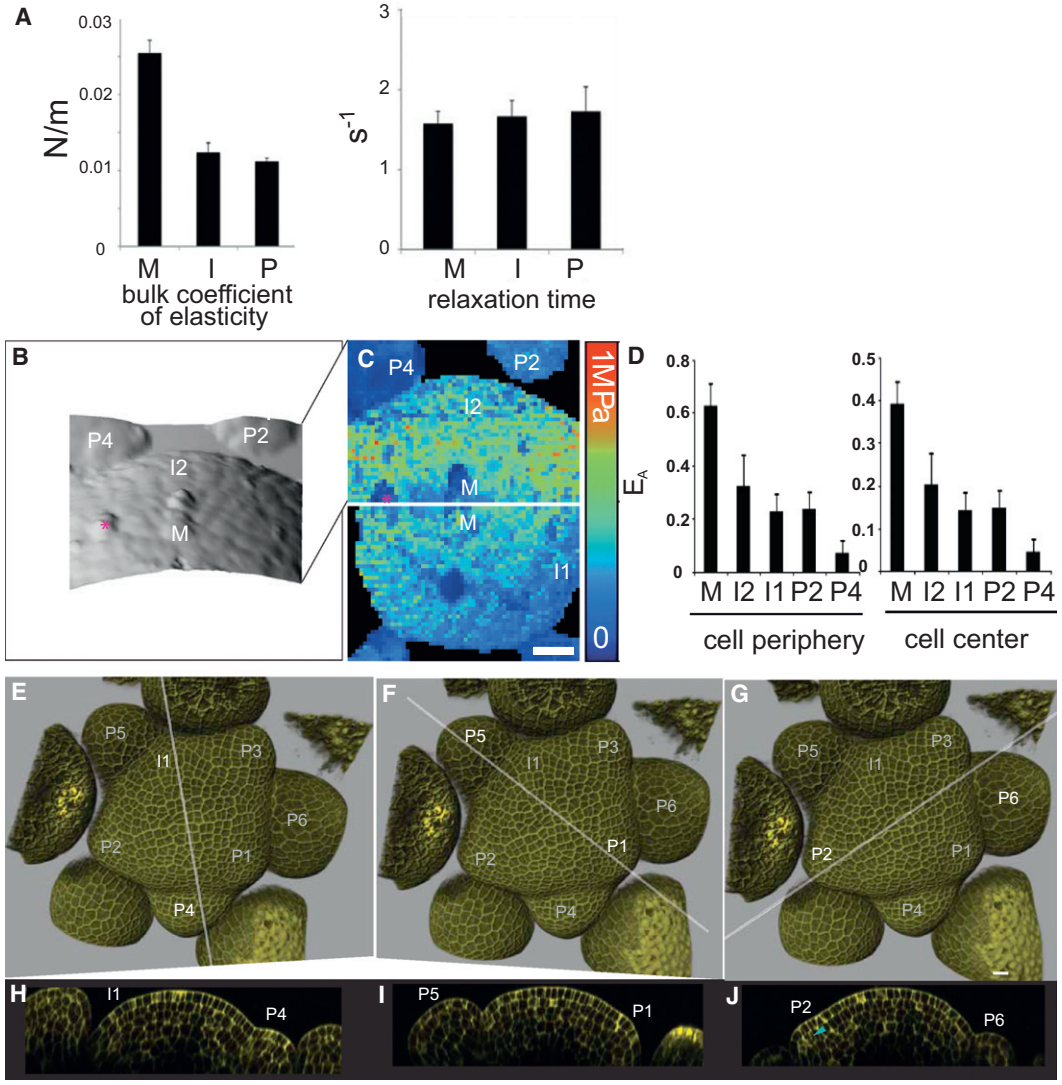

Figure 1. Composite Cell Wall Mechanics in the *Arabidopsis* Shoot Apical Meristem

(A) The mean and the standard deviation of the bulk coefficient of elasticity (left) and the associated relaxation time (right) measured on meristem dome, incipient organ, and primordia (P3 onward) at five different points each.

(B) Topographical reconstruction of an *Arabidopsis* inflorescence meristem from atomic force microscopy (AFM) point-of-contact data obtained with a 5 μm bead. Protruding cells correlate with areas of markedly reduced stiffness (red asterisk in B and C). The topographical reconstruction is 60 μm wide and up to 15 μm high.

(C) Representative map of the apparent Young's modulus (E_A) of the same meristem as in (A), showing differences in E_A (representative of 36 studied; Figure S1). The map shows data from two successive maps of 45 × 64 and 40 × 64 force scans. In this and all other such panels, E_A maps are presented as heat maps with their respective scales.

(D) Graph representing the E_A of the meristem in (A) and (B), distinguishing the areas corresponding to cell periphery and cell center.

(E–J) Confocal stack of an *Arabidopsis* inflorescence meristem stained with propidium iodide, illustrating phyllotactic pattern, surface topography, and cell size in I1 (E), P1 (F), and P2 (G). Virtual sections of (E)–(G) are shown in (H)–(J). Blue arrowhead indicates L2 division in P2. White text indicates primordia or incipient primordia shown in virtual sections (H)–(J).

Each pixel in the E_A map represents the E_A calculated from a single force-indentation curve, and each map consists of 4,096 data points. The E_A plotted on the graphs was determined by sampling data points within the area of interest (see Experimental Procedures and Supplemental Experimental Procedures). The following abbreviations are used: P: primordia; I, incipient organ; M, meristem dome. Error bars indicate standard deviation (SD) of measurements. Scale bars represent 10 μm.

Using a 5 μm bead tip, we observed that *PME5oe* meristems and peripheral zones (Pe) had a uniform lower E_A, similar to that of nontransgenic (NT) control primordia, whereas *PMEI3oe* meristems and Pe had a uniform higher E_A, similar to that of the NT meristem (Figures 2C–2E). The differences in E_A between NT, *PME5oe*, and *PMEI3oe* occurred irrespective of cell geometry (compare Figures 1E–1J to Figures 2F–2I and Figure S2). These data show that changes in pectin methylesterification status have effects on cell wall mechanics and that these effects correlate well with the downstream effects on organ initiation.

Decreases in E_A at Incipient Primordia Are Initiated in Underlying Tissue Layers and Not in the L1

In *Arabidopsis*, the shoot apical meristem is organized in distinct tissue layers: an outer epidermis (or L1 layer), an

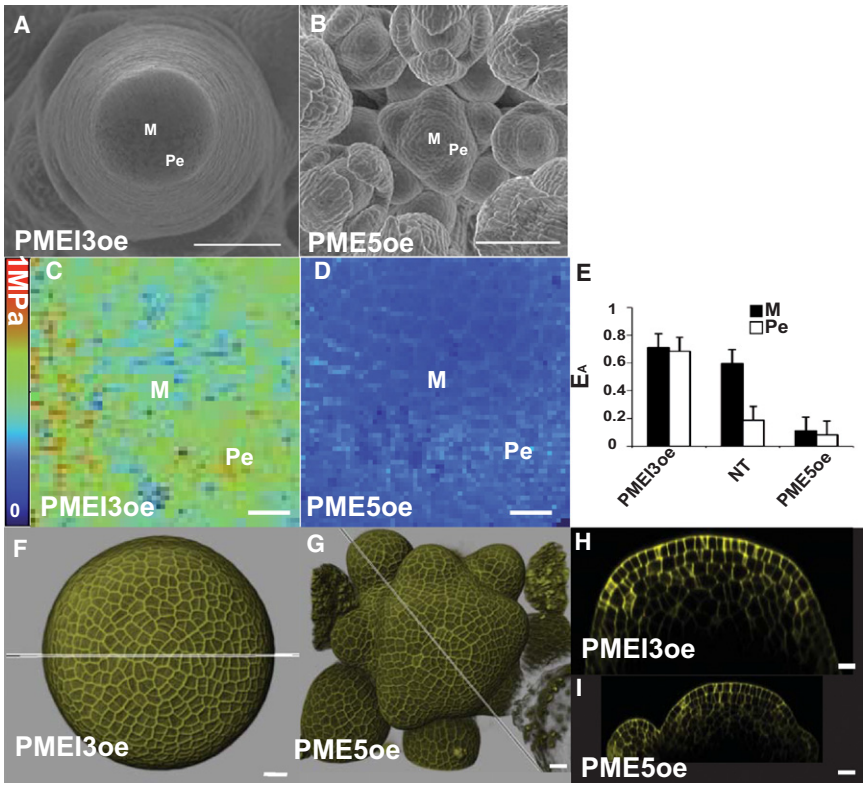

Figure 2. Effect of Pectin Modifications on Mechanical Properties in the Meristem and Phyllotaxis

(A and B) Scanning electron micrographs of transgenic meristems overexpressing the *PECTIN METHYLESTERASE INHIBITOR 3* (*PMEI3oe*) or *PECTIN METHYLESTERASE 5* (*PME5oe*) genes, respectively.

(C–E) E_A maps (C and D) and graph (E) of representative *PMEI3oe* and *PME5oe* meristems (representative of the 8 and 13 studied; Figure S5).

(F–I) Confocal stacks of *PMEI3oe* (F and H) and *PME5oe* (G and I) meristems showing surface topography and cell size in meristem and periphery.

Scale bars represent 100 μm in (A) and (B) and 10 μm in all other panels. The following abbreviations are used: M, meristem dome; Pe, meristem periphery. Note that meristems in (A) and (B), (C) and (D), and (F)–(I) are different samples. Error bars indicate SD of measurements.

underlying L2 layer, and the multilayered L3 [10]. To determine in which cell layers the decrease in E_A occurred first, we used a modified version of an approach developed for animal tissues [24]. We used a 1 μm bead and a 5 μm bead as AFM probe tips to examine different tissue depths; based on cell size, a 1 μm bead would probe the properties of the L1, whereas a 5 μm bead would deform a larger volume, including subepidermal tissues (Figures 3E and 3F). Using the 1 μm bead tip on NT *Arabidopsis* inflorescence meristems, we observed a decreased E_A in emerged organs but, surprisingly, not at incipient organs (Figures 3B and 3C; Figure S3). Therefore, it is likely that the decrease in E_A in incipient organs, observed with the 5 μm probe, reflected changes in underlying tissues, not the L1. To determine when the first changes in E_A in the L1 layer occurred, we examined primordia of successive age, or plastochron, using a 1 μm bead (Figures 3G–3I). A significant decrease in E_A in the L1 was observed only from P2 or P3 on, concomitantly with the formation of a well-defined crease. We previously showed that demethylesterification of pectins in the L1 of primordia was only detectable from this particular stage onward [11] and therefore parallels the observed decrease in E_A. To confirm that spatial differences in E_A within the L1 did not play a role in organ initiation, we induced an E_A decrease specifically in the L1 layer by expressing the *PME5* gene under control of an inducible form of the L1-specific *AtML1* promoter (*L1-PME5oe*; Figure S3). AFM measurements with a 1 μm probe on induced *L1-PME5oe* meristems showed an overall decrease of E_A in the L1, and emerged organs could not be distinguished from the meristem (Figures 3J–3L; Figure S3). Measurements with a 5 μm probe also showed a lower overall E_A, but differential E_A between areas was maintained (Figures 3M–3O; Figure S3). The L1-specific decreases in E_A (in *L1-PME5oe*) did not lead to aberrant organ positioning, whereas a decrease in all layers (in *PME5oe*) did (Figure S3). In sum, our results reveal a causal link between pectin demethylesterification and a decrease in E_A and suggest that the decrease in E_A in subepidermal layers is the first mechanical event underlying primordia initiation.

Discussion

In this study, we present measurements of the elastic response of cell walls, represented by E_A. It is not clear how the elasticity of the wall relates to its extensibility, which is a measure of the irreversible deformation over time associated with growth [18]. Although viscoelasticity has been correlated with growth in several studies [25, 26], such a correlation may not be a prerequisite in all contexts [18]. Here and in a previous study [11], we have shown that manipulating the E_A of the cell wall has an impact on organ initiation and therefore presumably wall extensibility. The exact mechanism underlying this link remains to be determined: the decrease in E_A may reflect increased cell wall hydration [27], which in turn may facilitate the sliding of wall polymers or the mobility of wall-modifying agents (expansins, XTH) and thus increase extensibility [28–30]. In vivo measurements of wall hydration and/or thickness during organ initiation may clarify this.

Our results indicate that pectin modification is one major contributor to wall elasticity within the meristem. The correlation between a decrease in E_A and pectin demethylesterification was unexpected, given the widely accepted model that predicts cell wall stiffening upon PME activity [23] (see Supplemental Experimental Procedures for a more detailed discussion).

Organ emergence has been correlated with initial periclinal divisions (parallel to the surface) within the L2 and L3 layers, followed by anticlinal divisions (perpendicular to the surface) in the L1 layer [31–34]. This observation suggests that cell expansion is initiated in the L2 and L3 tissues and is consistent

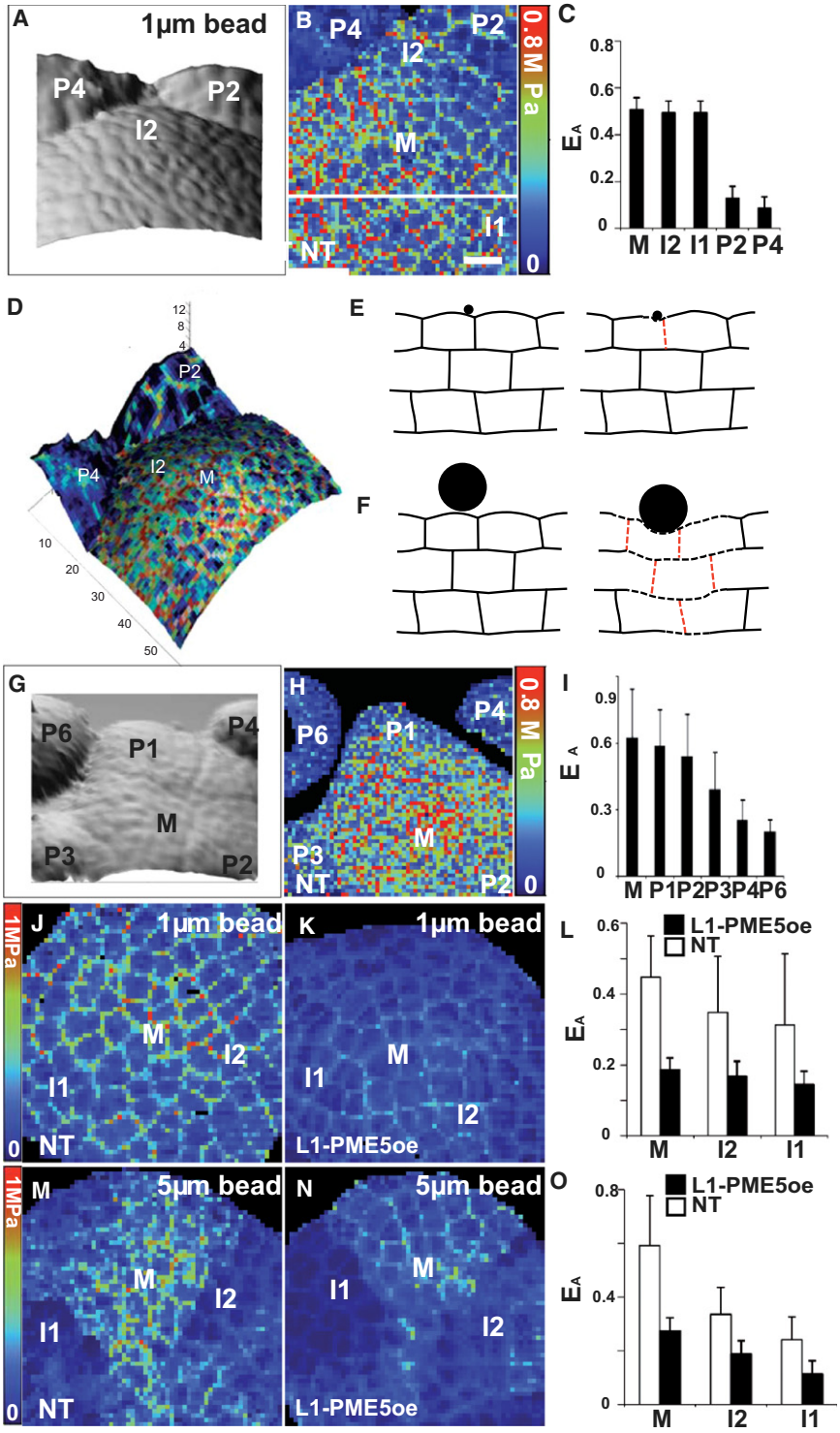

Figure 3. Cell Wall Mechanics in the L1 of the Meristem, and the Effect of L1-Only Softening

(A) Topographical reconstruction of an *Arabidopsis* inflorescence meristem from AFM point-of-contact data obtained with a 1 µm bead (same meristem as shown in Figures 1B and 1C).

(B and C) Representative E_A map (B; combination of two successive maps of 50 × 64 and 20 × 64 points) and graph (C) of the same meristem as in (A) and (B), showing differences in cell level mechanics and a higher cellular resolution (n = 11). Cross walls in emergent primordia are less obvious, due to the overall softening of these walls.

(D) Topographical reconstruction from (A) with imposed E_A map data from (B) to show sample dimensions and the nonexistent correlation between geometry and E_A variation.

(E and F) Theoretical representations of tissue level specificity given by different probe sizes. The range of volumetric compression was obtained using a 1 µm bead (E) and a 5 µm bead (F).

(G–I) Topographical reconstruction (G), E_A map (H), and E_A graph (I) from a representative meristem showing successive primordia in time from I1 to P3. Note that P2 stage primordium here is less developed than that in (A) and (D), as indicated by the degree of bulging.

(J, L, M, and O) E_A maps (J and M) and corresponding graphs (L and O) of nontransgenic control meristems for comparison (n = 12 and n = 36, respectively).

(K, L, N, and O) E_A maps (K and N) and corresponding graphs (L and O) of transgenic plants (K and N) expressing the inducible *PME5* gene in L1 (*L1-PME5oe*; n = 6), 18 hr after induction, probed with a 1 µm bead and a 5 µm bead, respectively.

All graphed E_A data were taken from anticlinal cell walls (see Experimental Procedures and Supplemental Experimental Procedures). Scale bars represent 10 µm. Error bars indicate SD of measurements.

with Sachs' theory that growth is driven by inner layers [35]. In contrast, it has also been suggested that the epidermis may restrict growth [36], as shown in aerial parts of the plant [37, 38]. The latter assumption also underlies recent mathematical models, which reduce the meristem to an inflated elastic shell with no significant mechanical contribution of internal tissues [7, 8, 39]. Here we have demonstrated that the first decreases in E_A are seen subepidermally (L2 and L3) at incipient sites, whereas a decrease in E_A in the L1 was observed only when a more complex geometry emerged (>P2–P3), as shown by the formation of a crease. These results suggest that the decrease in E_A of underlying tissues triggers cell expansion and division and thus provides the driving force for the surface deformation (Figure 4). We propose that the L1 layer only becomes growth-limiting once the organ has been initiated.

Over the past decade, it has become clear that maxima of the phytohormone auxin are essential for organ positioning and formation (Figure 4) [10, 40, 41]. Auxin is tightly linked to the mechanics of the meristem: auxin maxima affect expansin activity, and recent work has shown that the auxin transporter PIN1 responds to mechanical stresses [8]. Auxin maxima at incipient sites overlap with changes in pectin chemistry and E_A; future investigation of the relationship between auxin and pectin modification will prove critical for our understanding of organ formation.

Within this work, we have shown the importance of examining cell wall mechanics with respect to growth. Our methods

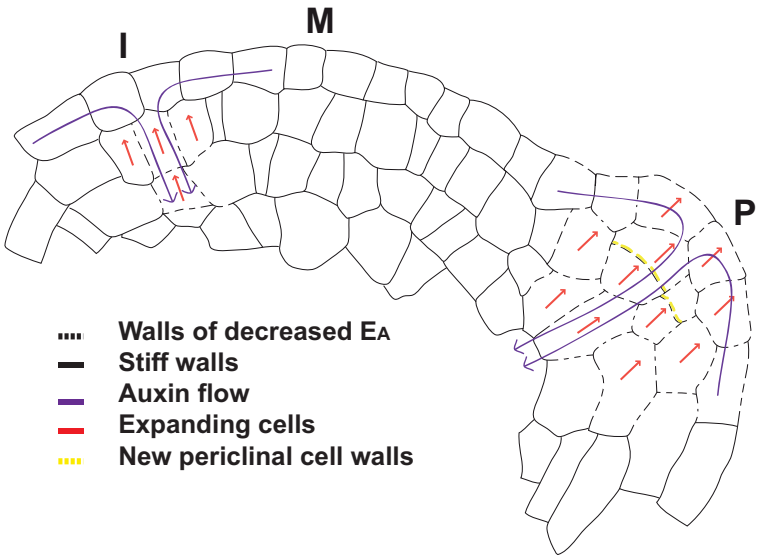

Figure 4. Organogenesis in *Arabidopsis* from a Mechano-chemical Perspective

Representation of an *Arabidopsis* inflorescence meristem. Auxin flow creates maxima at incipient organ sites; purple arrows show the direction of auxin flow in the outer epidermal layer (L1) as well as the channeling down of auxin at the convergence point. At these positions, localized de-methylesterification of pectins in the cell walls occurs, which contributes to increases in wall elasticity (a decrease in the apparent Young's modulus, E_A). The decrease in E_A is the first observable mechanical event associated with cell expansion driving organ emergence (red arrows). At the site of an incipient organ (I), the decrease in E_A is detected only in the underlying tissues, not in the epidermal layer, illustrating that the increase in wall elasticity occurs first in subepidermal layers. Within an emerged organ (P), the walls of all cells have a lower E_A, which is correlated with the increased growth rate of these cells. The decrease in E_A in underlying tissues first could lead to periclinal divisions in the L2 (yellow lines) as it diverges from a distinct monolayer of cells into a more complex tissue. Within the meristem dome (M), all cells appear to have relatively stiffer walls.

have enabled a literal "in-depth" look at the cell mechanics associated with organ formation. The results presented here support a model in which subepidermal tissues play an important mechanical role in organ initiation, and epidermal tissues in regulating subsequent growth. The key role of pectin modifications in the regulation of cell wall mechanics during organ formation has been highlighted. AFM-based techniques most likely will continue to provide crucial insights into the mechanics of growth and development in plants.

Experimental Procedures

Plant Material and Growth Conditions

Arabidopsis thaliana plants were grown in controlled chambers under short-day or long-day conditions, as described previously [11]. The *PME5oe* and *PMEI3oe* transgenic *Arabidopsis* plants have been described elsewhere [12]. The *L1-PME5oe* lines were generated by transforming plants containing *pAtML1-AlcR* with the *pAlcA-PME5* construct [12]. Ten independent *L1-PME5oe* lines were obtained. Three of these lines were used for the study of phyllotactic modifications and for the immunolabeling of demethylesterified HG (Figure S3), and one line was used for AFM and confocal analysis. These lines also expressed *pAlcA-GFP*, and this marker was restricted to the L1 (data not shown).

Scanning Electron Microscopy

Images were obtained with an S-3500N variable-pressure scanning electron microscope (Hitachi).

Confocal Microscopy

A. thaliana meristems were dissected from nontransgenic, induced *35S:PMEI3*, and induced *35S:PME5* plants and stained in 0.05% propidium iodide for visualization of cell walls. Transgenic plants were induced for 48 hr as described [11, 42]. Confocal stacks were taken of 12 meristems per genotype, using a 63× long-distance water immersion lens attached to a Leica DMR XE7 as described in [43]. Samples were mounted in water, and 0.5 μm deep optical sections were taken to cover the depth of the meristem and youngest primordia. Resulting image stacks were processed using Imaris software (V6) to obtain surface projections and slices through different staged organs and the meristem. Images in figures are representative of all samples examined (n = 12 per genotype).

AFM Measurements

All samples were plasmolyzed in 10% (0.55 M) mannitol prior to measurement. This treatment was fully reversible and did not affect the viability of the meristem (data not shown). The following numbers of meristems were analyzed: NT, n = 36 (5 μm beads) and n = 12 (1 μm beads); *PMEI3oe*, n = 8; *PME5oe*, n = 13; *L1-PME5oe*, n = 8.

For E_A measurement using force spectroscopy, an approach and retract period of 0.3 s with no delay was used and a constant maximum force was imposed; this value was determined for each experiment to obtain a maximum deformation at all points of the sample of about 500 nm (10% deformation of a meristematic L1 cell in *Arabidopsis*).

To evaluate the viscoelasticity of meristem tissue, we performed three to four successive long indentation cycles (10 s indentation followed by 10 s partial release). An initial indentation of ~0.5–1 μm was followed by cyclical indentation and releases of 0.25 μm for at least three cycles. In the indentation portion force was kept constant, and in the release portion deformation was constant.

Viscosity Calculations

Our modified Kelvin-Voigt model yields the following equation:

$$F(t) = a\frac{dx}{dt}\left(1 - e^{-bt}\right), \quad (1)$$

where

$$b = \frac{k_1 + k_2}{\eta} \quad (2)$$

and

$$a = \frac{k_1 k_2}{k_1 + k_2}. \quad (3)$$

Although we could not solve k_1 and k_2 from the model, we could gain the bulk elasticity, a, and also determine the relaxation time, b. We focused on the part of the experiment where the deformation was kept constant, where the model predicts that the force will evolve as a negative exponential. MATLAB (http://www.mathworks.com/products/matlab/) was used to fit the data using the above Equations 1–3.

Indentation cycles were performed at several positions on the meristem, incipient organs, and primordia. The meristem, incipient organs, and primordia were determined following an initial AFM elasticity mapping. The average value of a and b is presented for each point of measurement for four meristems.

Apparent Young's Modulus Calculations

The Hertzian contact model [22] provides the relationship between the force applied, F, and the resulting indentation, δ:

$$F = \lambda\delta^{\beta} = A\frac{E}{1 - \nu^2}\delta^{\beta}. \quad (4)$$

Exponent β and shape factor A depend on the precise bead shape (see Table 1 in [22]). E is the Young's modulus (herein referred to as apparent Young's modulus, E_A) and ν the Poisson ratio (assumed $\nu \approx 0.5$).

Based on E_A maps, 30–40 individual E_A values were taken along anticlinal walls, or their predicted area, and averaged to provide graphical data. The total number of values displayed in graphs corresponds to 50% or 25% of the total values available.

Incipient organ position was determined by extrapolating the phyllotactic pattern, and the ten cells surrounding this position were considered to be included within it.

Supplemental Information

Supplemental Information includes three figures and Supplemental Experimental Procedures and can be found with this article online at doi:10.1016/j.cub.2011.08.057.

Acknowledgments

We give special thanks to Yves Couder for many helpful discussions and reading of the manuscript. We thank Atef Asnacios for the calibration of the cantilevers and discussion, Gregory Mouille for discussion, Anne Dupras for providing free access to AFM microscopy at the outset of the project, Pierre Van Cutsem for providing the 2F4 antibodies, and Cyprien Gay for help with our viscoelasticity model. This work was funded in part by Human Frontier Science Program grant RGP0062/2005-C; the European Union FP6 project "Agron-Omics"; the Agence Nationale de la Recherche projects ANR-08-BLAN-0292 ("Wallintegrity"), "Growpec," and "Mechastem"; the Swiss National Science Foundation; and SystemsX.ch, the Swiss Initiative in Systems Biology. S.A.B. is funded by a US National Science Foundation International Research Fellowship (award OISE-0853105).

Received: July 25, 2011
Revised: August 23, 2011
Accepted: August 25, 2011
Published online: October 6, 2011

References

1. Müller, D.J., and Dufrêne, Y.F. (2011). Force nanoscopy of living cells. Curr. Biol. *21*, R212–R216.
2. Desprat, N., Supatto, W., Pouille, P.A., Beaurepaire, E., and Farge, E. (2008). Tissue deformation modulates twist expression to determine anterior midgut differentiation in Drosophila embryos. Dev. Cell *15*, 470–477.
3. Pouille, P.A., Ahmadi, P., Brunet, A.C., and Farge, E. (2009). Mechanical signals trigger Myosin II redistribution and mesoderm invagination in Drosophila embryos. Sci. Signal. *2*, ra16.
4. Al-Kilani, A., Lorthois, S., Nguyen, T.H., Le Noble, F., Cornelissen, A., Unbekandt, M., Boryskina, O., Leroy, L., and Fleury, V. (2008). During vertebrate development, arteries exert a morphological control over the venous pattern through physical factors. Phys. Rev. E Stat. Nonlin. Soft Matter Phys. *77*, 051912.
5. Mirabet, V., Das, P., Boudaoud, A., and Hamant, O. (2011). The role of mechanical forces in plant morphogenesis. Annu. Rev. Plant Biol. *62*, 365–385.
6. Uyttewaal, M., Traas, J., and Hamant, O. (2010). Integrating physical stress, growth, and development. Curr. Opin. Plant Biol. *13*, 46–52.
7. Hamant, O., Heisler, M.G., Jönsson, H., Krupinski, P., Uyttewaal, M., Bokov, P., Corson, F., Sahlin, P., Boudaoud, A., Meyerowitz, E.M., et al. (2008). Developmental patterning by mechanical signals in Arabidopsis. Science *322*, 1650–1655.
8. Heisler, M.G., Hamant, O., Krupinski, P., Uyttewaal, M., Ohno, C., Jönsson, H., Traas, J., and Meyerowitz, E.M. (2010). Alignment between PIN1 polarity and microtubule orientation in the shoot apical meristem reveals a tight coupling between morphogenesis and auxin transport. PLoS Biol. *8*, e1000516.
9. Boudaoud, A. (2010). An introduction to the mechanics of morphogenesis for plant biologists. Trends Plant Sci. *15*, 353–360.
10. Braybrook, S.A., and Kuhlemeier, C. (2010). How a plant builds leaves. Plant Cell *22*, 1006–1018.
11. Peaucelle, A., Louvet, R., Johansen, J.N., Höfte, H., Laufs, P., Pelloux, J., and Mouille, G. (2008). Arabidopsis phyllotaxis is controlled by the methylesterification status of cell-wall pectins. Curr. Biol. *18*, 1943–1948.
12. Cosgrove, D.J. (1993). How do plant cell walls extend? Plant Physiol. *102*, 1–6.
13. Schopfer, P. (2006). Biomechanics of plant growth. Am. J. Bot. *93*, 1415–1425.
14. Fleming, A., McQueen-Mason, S., Mandel, T., and Kuhlemeier, C. (1997). Induction of leaf primordia by the cell wall protein expansin. Science *276*, 1415–1418.
15. Cosgrove, D.J. (2000). Expansive growth of plant cell walls. Plant Physiol. Biochem. *38*, 109–124.
16. Dick-Perez, M., Zhang, Y., Hayes, J., Salazar, A., Zabotina, O.A., and Hong, M. (2011). Structure and interactions of plant cell-wall polysaccharides by two- and three-dimensional magic-angle-spinning solid-state NMR. Biochemistry *50*, 989–1000.
17. Kerstens, S., Decraemer, W.F., and Verbelen, J.P. (2001). Cell walls at the plant surface behave mechanically like fiber-reinforced composite materials. Plant Physiol. *127*, 381–385.
18. Cosgrove, D.J. (1993). Wall extensibility: its nature, measurement and relationship to plant cell growth. New Phytol. *124*, 1–23.
19. Kwiatkowska, D. (2004). Surface growth at the reproductive shoot apex of Arabidopsis thaliana pin-formed 1 and wild type. J. Exp. Bot. *55*, 1021–1032.
20. Kwiatkowska, D. (2006). Flower primordium formation at the Arabidopsis shoot apex: quantitative analysis of surface geometry and growth. J. Exp. Bot. *57*, 571–580.
21. Reddy, G.V., Heisler, M.G., Ehrhardt, D.W., and Meyerowitz, E.M. (2004). Real-time lineage analysis reveals oriented cell divisions associated with morphogenesis at the shoot apex of Arabidopsis thaliana. Development *131*, 4225–4237.
22. Lin, D.C., Dimitriadis, E.K., and Horkay, F. (2007). Robust strategies for automated AFM force curve analysis—I. Non-adhesive indentation of soft, inhomogeneous materials. J. Biomech. Eng. *129*, 430–440.
23. Pelloux, J., Rustérucci, C., and Mellerowicz, E.J. (2007). New insights into pectin methylesterase structure and function. Trends Plant Sci. *12*, 267–277.
24. Stolz, M., Raiteri, R., Daniels, A.U., VanLandingham, M.R., Baschong, W., and Aebi, U. (2004). Dynamic elastic modulus of porcine articular cartilage determined at two different levels of tissue organization by indentation-type atomic force microscopy. Biophys. J. *86*, 3269–3283.
25. Kutschera, U. (1996). Cessation of cell elongation in rye coleoptiles is accompanied by a loss of cell-wall plasticity. J. Exp. Bot. *47*, 1387–1394.
26. Nolte, T., and Schopfer, P. (1997). Viscoelastic versus plastic cell wall extensibility in growing seedling organs: A contribution to avoid some misconceptions. J. Exp. Bot. *48*, 2103–2107.
27. Caesar, K., Elgass, K., Chen, Z., Huppenberger, P., Witthöft, J., Schleifenbaum, F., Blatt, M.R., Oecking, C., and Harter, K. (2011). A fast brassinolide-regulated response pathway in the plasma membrane of Arabidopsis thaliana. Plant J. *66*, 528–540.
28. Durachko, D.M., and Cosgrove, D.J. (2009). Measuring plant cell wall extension (creep) induced by acidic pH and by alpha-expansin. J. Vis. Exp. *2009*, 1263.
29. Van Sandt, V.S., Suslov, D., Verbelen, J.P., and Vissenberg, K. (2007). Xyloglucan endotransglucosylase activity loosens a plant cell wall. Ann. Bot. (Lond.) *100*, 1467–1473.
30. Ryden, P., Sugimoto-Shirasu, K., Smith, A.C., Findlay, K., Reiter, W.D., and McCann, M.C. (2003). Tensile properties of Arabidopsis cell walls depend on both a xyloglucan cross-linked microfibrillar network and rhamnogalacturonan II-borate complexes. Plant Physiol. *132*, 1033–1040.
31. Cronshaw, J., and Esau, K. (1968). Cell division in leaves of Nicotiana. Protoplasma *65*, 1–24.
32. Morag, E.C., and Lyndon, R.F. (1996). The relationship between the distribution of periclinal cell divisions in the shoot apex and leaf initiation. Ann. Bot. *56*, 737–746.
33. Lyndon, R.F., and Cunninghame, M.E. (1986). Control of shoot apical development via cell division. Symp. Soc. Exp. Biol. *40*, 233–255.
34. Tepfer, S.S. (1960). The shoot apex and early leaf development in Clematis. Am. J. Bot. *47*, 655–664.
35. Sachs, T. (1972). A possible basis for apical organization in plants. J. Theor. Biol. *37*, 353–361.
36. Green, P.B. (1999). Expression of pattern in plants: combining molecular and calculus-based biophysical paradigms. Am. J. Bot. *86*, 1059–1076.
37. Savaldi-Goldstein, S., and Chory, J. (2008). Growth coordination and the shoot epidermis. Curr. Opin. Plant Biol. *11*, 42–48.
38. Savaldi-Goldstein, S., Peto, C., and Chory, J. (2007). The epidermis both drives and restricts plant shoot growth. Nature *446*, 199–202.

39. Merks, R.M., Guravage, M., Inzé, D., and Beemster, G.T. (2011). VirtualLeaf: an open-source framework for cell-based modeling of plant tissue growth and development. Plant Physiol. *155*, 656–666.
40. Reinhardt, D., Mandel, T., and Kuhlemeier, C. (2000). Auxin regulates the initiation and radial position of plant lateral organs. Plant Cell *12*, 507–518.
41. Reinhardt, D., Pesce, E.R., Stieger, P., Mandel, T., Baltensperger, K., Bennett, M., Traas, J., Friml, J., and Kuhlemeier, C. (2003). Regulation of phyllotaxis by polar auxin transport. Nature *426*, 255–260.
42. Deveaux, Y., Peaucelle, A., Roberts, G.R., Coen, E., Simon, R., Mizukami, Y., Traas, J., Murray, J.A., Doonan, J.H., and Laufs, P. (2003). The ethanol switch: a tool for tissue-specific gene induction during plant development. Plant J. *36*, 918–930.
43. Bayer, E.M., Smith, R.S., Mandel, T., Nakayama, N., Sauer, M., Prusinkiewicz, P., and Kuhlemeier, C. (2009). Integration of transport-based models for phyllotaxis and midvein formation. Genes Dev. *23*, 373–384.